Effects of thermal cycles on soil behaviour: theoretical and experimental studies

Charles W. W. Ng[1*], *Chao* Zhou[2], *Shuai* Zhang[1], and *Qi* Zhang[1]

[1]Hong Kong University of Science and Technology, Hong Kong, China
[2]Hong Kong Polytechnical University, Hong Kong, China

Abstract. Fundamental understanding and proper modelling of soil behaviour under thermal cycles are increasingly important and essential for the analysis and design of many emerging infrastructures, such as geothermal structures and embankment-atmosphere interactions under a changing climate. Previous studies mainly focus on monotonic thermal loading of thermo-mechanical behaviour of soils. Based on a unified, state-dependent theoretical framework in the form of compliance matrix, a new constitutive model is developed to simulate the cyclic thermo-mechanical behaviour of saturated and unsaturated soils. This new bounding surface model is formulated in terms of Bishop's stress and suction. Apart from the loading and bounding surfaces, a memory surface is incorporated in the model to simulate cyclic thermal behaviour of soils. To verify the new model, computed results are compared with measured data from cyclic heating-cooling tests on saturated and unsaturated soils at various suctions. Based on this new model, two engineering applications are analysed including cyclic thermally loaded floating energy pile foundations and a deep excavation in the unsaturated ground. Consistent results are obtained between computed and measured data.

1 Introduction

Soil is a porous medium in which the pores between solid grains play an important role in governing its mechanical, hydraulic and thermal behaviour [1-3]. The pores can be filled with liquid and/or gas either fully or partially. Many classical theories of soil mechanics developed assuming that the pores are filled up with either liquid (i.e., fully saturated) or gas (i.e., completely dry), e.g., the Terzaghi's theory of one-dimensional consolidation. However, fully saturated and completely dry states are only two limiting conditions of soils [2]. In numerous geotechnical engineering applications, the degree of saturation in soils lies between 0% and 100%. Many key phenomena observed in unsaturated soils cannot be explained adequately by the classical theories of soil mechanics, leading to the substantial amount of research and significant advancements of unsaturated soil mechanics over the past few decades (e.g., [2, 4-27]).

Since the pioneering work in the 1950s and 1960s to develop different laboratory techniques to control suction and test unsaturated soils [28-38], the contributions of suction to the mechanical and hydraulic behaviour of unsaturated soils have been much better understood. The constitutive modelling of unsaturated soil behaviour has also been greatly improved in the past three decades [4-27]. The existing constitutive models for unsaturated soils have been discussed in several review papers [3, 39-46]. In particular, Ng et al. [3] reviewed existing research work in the literature and formulated a unified and state-dependent constitutive framework for unsaturated soils. Within this constitutive framework, the modelling of state-dependent behaviour of unsaturated soils was discussed in a systematic approach. It should be pointed out that most of the existing models concentrated on isothermal conditions. Also previous studies of the thermo-mechanical behaviour of soil mainly focus on monotonic thermal loading. Under a changing climate, fundamental understanding and proper modelling of soil behaviour under thermal cycles are urgently needed for analysing and designing many emerging infrastructures such as geothermal structures and embankment.

In this lecture, based on the constitutive framework of Ng et al. [3], a newly developed state-dependent cyclic thermo-hydro-mechanical model is introduced for simulating unsaturated soils. This new model is verified using advanced laboratory tests, such as cyclic heating-cooling tests on saturated and unsaturated soils. Based on the theoretical and experimental studies, two geotechnical engineering applications (i.e., floating energy pile foundations and deep excavation in the unsaturated ground) are analysed. Key deformation mechanisms are revealed and explained. It should be noted that some contents of this lecture are based on and extracted directly from Ng et al. [3, 47, 48].

* Corresponding author: cecwwng@ust.hk

2 A unified and state-dependent theoretical framework for modelling the behaviour of unsaturated soils

2.1 Description of state-dependent theoretical framework

In the constitutive modelling of unsaturated soils, one of the key issues is the choice of proper constitutive variables. Many different constitutive variables have been proposed in the literature to model the mechanical behaviour of unsaturated soils (e.g., [12, 49, 50]). Gens et al. [40] reviewed the different variables adopted in existing elastoplastic models. They believed that "*Different constitutive stresses stand on an equal footing and the matter of adopting one or the other must be decided using the criteria of convenience*." In the unified and state-dependent theoretical framework of this current study, net stress and matric suction are used for simplicity. Net stress is defined as the difference between total stress (σ) and pore air pressure (u_a). Matric suction is calculated as the difference between pore air and pore water pressures (u_w), and it is referred to as suction for simplicity in the following paragraphs.

By adopting net stress and suction, the constitutive formulations for an unsaturated soil can be expressed in a general incremental form as follows:

$$\begin{bmatrix} \mathrm{d}\varepsilon_\mathrm{v} \\ \mathrm{d}\varepsilon_\mathrm{q} \\ \mathrm{d}S_\mathrm{r} \end{bmatrix} = \begin{bmatrix} I_{11} & I_{12} & I_{13} \\ I_{21} & I_{22} & I_{23} \\ I_{31} & I_{32} & I_{33} \end{bmatrix} \begin{bmatrix} \mathrm{d}p \\ \mathrm{d}q \\ \mathrm{d}s \end{bmatrix} \quad (1)$$

where $\mathrm{d}\varepsilon_\mathrm{v}$ is the increment in volumetric strain; $\mathrm{d}\varepsilon_\mathrm{q}$ is the increment in deviator strain; $\mathrm{d}S_\mathrm{r}$ is the increment in the degree of saturation; $\mathrm{d}p$ is the increment in the mean net stress; $\mathrm{d}q$ is the increment in the deviator stress; $\mathrm{d}s$ is the increment in suction; and I_{ij} (i = 1, 2 and 3; j = 1, 2 and 3) are state-dependent variables for a given soil. According to equation (1), the variables I_{11}, I_{21}, and I_{31} in the compliance matrix describe the behaviour of unsaturated soils during compression, including the development of volumetric strain, deviator strain and degree of saturation. Similarly, I_{12}, I_{22}, and I_{32} describe the hydro-mechanical behaviour during the shearing process, while I_{13}, I_{23} and I_{33} capture the behaviour of soil subjected to drying/wetting. All nine variables can be calibrated through suction- and stress-controlled tests on unsaturated soils. These variables can be also determined by using constitutive formulations for the compression, shearing and water retention behaviour of unsaturated soils, as discussed later. Equation (1) is still valid when soil is saturated, which is considered as a special case of unsaturated soil with S_r = 100%. At this special condition, the net stress is replaced by the Terzaghi's effective stress and the values of I_{13}, I_{23}, I_{31}, I_{32} and I_{33} become zero.

Some unsaturated soil models in the literature are based on other constitutive stress variables rather than net stress and suction. These models can be also converted to equation (1) by matrix transformation. In any constitutive model, the relationship between strain increment $\{\mathbf{d\hat{\varepsilon}}\}$ and stress increment $\{\mathbf{d\hat{\sigma}}^*\}$ can be described using a general formulation:

$$\{\mathrm{d}\hat{\boldsymbol{\varepsilon}}\} = [\boldsymbol{C}*]\{\mathrm{d}\hat{\boldsymbol{\sigma}}*\} \quad (2)$$

where $[\mathbf{C}^*]$ is the compliance matrix; $\{\hat{\boldsymbol{\sigma}}^*\}$ and $\{\hat{\boldsymbol{\varepsilon}}\}$ are the constitutive stress and strain variables, respectively. For the discussion here, the strain variables $\{\hat{\boldsymbol{\varepsilon}}\}$ is defined as $\{\varepsilon_v, \varepsilon_q, S_r\}$ in all models. To obtain the relationship between $[\mathbf{C}^*]$ and $[\mathbf{C}]$ (i.e., the compliance matrix defined in equation (1)), $\{\mathrm{d}\hat{\boldsymbol{\sigma}}^*\}$ can be expressed as [51]

$$\{\mathrm{d}\hat{\boldsymbol{\sigma}}^*\} = [\boldsymbol{T_a}]\{\mathrm{d}\hat{\boldsymbol{\sigma}}\} + [\mathbf{T_b}]\{\mathrm{d}\hat{\boldsymbol{\varepsilon}}\} \quad (3)$$

where $\{\mathrm{d}\hat{\boldsymbol{\sigma}}\}$ is the incremental form of constitutive stress variables $\{\mathrm{d}p, \mathrm{d}q, \mathrm{d}s\}$ used in equation (1); $[\mathbf{T_a}]$ and $[\mathbf{T_b}]$ are two matrixes and their values depend on the constitutive stress variables in the constitutive model investigated. Substituting equations (1) and (3) into equation (2), it is obtained that

$$[\boldsymbol{C}] = [\boldsymbol{I} - \boldsymbol{C}^*\boldsymbol{T_b}]^{-1}[\boldsymbol{C}^*][\boldsymbol{T_a}] \quad (4)$$

where $[\mathbf{I}]$ is a unit matrix. It should be noted that equations (2) and (4) are general equations. They can be used to convert any constitutive model to equation (1). When different models are used, however, $[\mathbf{T_a}]$ and $[\mathbf{T_b}]$ take different forms. For example, the model of Wheeler et al. [12] uses the following three constitutive stress variables: $\{\hat{\boldsymbol{\sigma}}^*\} = \{p^*, q, s^*\}$, where the Bishop's stress p^* and modified suction s^* are defined as $(p + sS_\mathrm{r})$ and (ns), respectively. From the incremental form of $\{\hat{\boldsymbol{\sigma}}^*\}$, it can be readily derived that:

$$[\boldsymbol{T_a}] = \begin{bmatrix} 1 & 0 & S_\mathrm{r} \\ 0 & 1 & 0 \\ 0 & 0 & n \end{bmatrix} \quad (5)$$

$$[\boldsymbol{T_b}] = \begin{bmatrix} 0 & 0 & s \\ 0 & 0 & 0 \\ (1-n)s & 0 & 0 \end{bmatrix} \quad (6)$$

Another example is the model of Khalili et al. [52], which adopts the following constitutive stress variables: $\{\hat{\boldsymbol{\sigma}}^*\} = \{p_\mathrm{k}^*, q, s\}$. p_k^* is the mean effective stress proposed by Khalili and Khabbaz [53]: $(p + \chi s)$, where χ is defined as follows:

$$\chi = \begin{cases} 1 & for\ s \le s_\mathrm{e} \\ \left(\dfrac{s}{s_\mathrm{e}}\right)^{-0.55} & for\ s > s_\mathrm{e} \end{cases} \quad (7)$$

where s_e is the suction value marking the transition between saturated and unsaturated states. $[\boldsymbol{T_a}]$ and $[\boldsymbol{T_b}]$ are calculated using the following two equations:

$$[\boldsymbol{T_a}] = \begin{bmatrix} 1 & 0 & 2(s/s_e)^{-0.55} \\ 0 & 1 & 0 \\ 0 & 0 & 1 \end{bmatrix} \quad (8)$$

$$[\boldsymbol{T_b}] = \begin{bmatrix} 0 & 0 & (s/s_e)^{0.45}(\partial s_e/\partial \varepsilon_v) \\ 0 & 0 & 0 \\ 0 & 0 & 0 \end{bmatrix} \quad (9)$$

Lu et al. [54] proposed a new effective stress formulation $(\sigma - \sigma^\mathrm{s})$ based on the concept of suction stress σ^s [55]. For constitutive models based on this effective stress formulation, $[\mathbf{T_a}]$ and $[\mathbf{T_b}]$ are calculated using the following two equations:

$$[\boldsymbol{T_a}] = \begin{bmatrix} 1 & 0 & (S_\mathrm{r} - S_\mathrm{rr})/(1 - S_\mathrm{rr}) \\ 0 & 1 & 0 \\ 0 & 0 & 1 \end{bmatrix} \quad (10)$$

$$[\boldsymbol{T}_{\mathbf{b}}] = \begin{bmatrix} 0 & 0 & (S_{\mathrm{r}} - S_{\mathrm{rr}})/(1 - S_{\mathrm{rr}}) \\ 0 & 0 & 0 \\ 0 & 0 & 0 \end{bmatrix} \quad (11)$$

where S_{rr} is the residual degree of saturation. The above three examples clearly show that all constitutive models can be converted to equation (1) by matrix transformation. Within this unified framework (i.e., equation (1)), the constitutive formulations for unsaturated soil behaviour are reviewed by Ng et al. [3].

2.2 State-dependent variables in compliance matrix

The formulations of all nine terms in equation (1) are briefly discussed below. The details of derivation can be found from Ng et al. [3].

The variable I_{11} in equation (1) can be expressed as below on the assumption that the compression behaviour of an unsaturated soil can be described by a straight line in the e-ln p plane [56]:

$$I_{11} = \frac{\alpha_{\mathrm{p}}(\mathrm{s})}{(1+e)p} \quad (12)$$

where e is the void ratio; $\alpha_{\mathrm{p}}(\mathrm{s})$ is the compressibility that is a function of suction. Equation (12) clearly reveals that the value of I_{11} is affected by net stress, suction and the void ratio. The state-dependent compressibility is considered by this equation and hence by equation (1).

The variable I_{12} in equation (1) can be derived based on the dilatancy formulation. When the state-dependent dilatancy of Chiu and Ng [56] is adopted, I_{12} is determined as follows:

$$I_{12} = (I_{22} - 1/G_0) d_1(\mathrm{s}) \left(\exp(m\psi) - \frac{\eta}{M}\right) \quad (13)$$

where G_0 is the elastic shear modulus; $d_1(\mathrm{s})$ and m are material parameters, and the former one is a function of suction; ψ is the state parameter [56, 57]; M is the gradient of critical state line in the plane of net mean stress (p') and deviator stress (q); η is the stress ratio (q/p'). According to equation (13), the value of I_{12} is affected by suction. Therefore, the state-dependent dilatancy of unsaturated soils is considered by this equation and hence by equation (1).

The variable I_{13} in equation (1) can be derived if the equation of Sheng et al. [58] is used to calculate the suction-induced volume change of unsaturated soils:

$$I_{13} = \frac{\lambda_{\mathrm{s}}}{(1+e)(p+s)} \quad (14)$$

where λ_{s} is the shrinkage index. A key feature of equation (14) is that the suction-induced volume changes of unsaturated soils are dependent on mean net stress. The coupling effects of hydro-mechanical behaviour are taken into account.

The variable I_{21} in equation (1) is mainly affected by the dilatancy during compression. Using the dilatancy equation of Chiu and Ng [56], I_{21}can be determined as below:

$$I_{21} = \frac{I_{11} - \kappa(\mathrm{s})/p}{\big(\lambda(\mathrm{s}) - \kappa(\mathrm{s})\big) d_2(\mathrm{s})\, M/\eta} \quad (15)$$

where $\kappa(\mathrm{s})$ is the swelling index; $d_2(\mathrm{s})$ is a material parameter that is a function of suction. It can be seen that the value of I_{21} is affected by suction. Therefore, the state-dependent dilatancy of unsaturated soils is considered by equation (15) and hence by equation (1).

The value of I_{22} depends on the current deviator strain (ε_{q}). When it is lower than the elastic threshold strain ($\varepsilon_{\mathrm{qe}}$), shear modulus is constant and it can be calculated using the equation of Ng and Yung [59]. Hence,

$$I_{22} = \frac{1}{C^2 f(\mathrm{e}) \left(\frac{p}{p_{\mathrm{r}}}\right)^{2n} \left(1 + \frac{s}{p_{\mathrm{r}}}\right)^{2k}} \quad (16a)$$

where C, n and k are material parameters; $f(\mathrm{e})$ is the void ratio function relating the dependence of the shear wave velocity to the void ratio; p_{r} is reference pressure.

When the current deviator strain is above the elastic threshold value, the strain dependence of shear modulus should be considered. If the formulation of Vardanega and Bolton [60] is used to model the strain-dependency of shear stiffness, I_{22} is calculated using the following equation:

$$I_{22} = \frac{1 + \left(\frac{\varepsilon_{\mathrm{q}} - \varepsilon_{\mathrm{qe}}}{\varepsilon_{\mathrm{qref}} - \varepsilon_{\mathrm{qe}}}\right)^{a}}{C^2 f(\mathrm{e}) \left(\frac{p}{p_{\mathrm{r}}}\right)^{2n} \left(1 + \frac{s}{p_{\mathrm{r}}}\right)^{2k}} \quad (16b)$$

where $\varepsilon_{\mathrm{qref}}$ is a characteristic reference strain, defined as the deviator strain at which secant shear modulus is reduced to $0.5G_0$; a is a material parameter.

The variable I_{23} in equation (1) can be derived:

$$I_{23} = \frac{I_{13}}{D_{\mathrm{s}}} - \frac{\alpha_{\mathrm{s}}}{D_{\mathrm{s}}(p+s)(1+e)} \quad (17)$$

where D_{s} is the dilatancy during drying/wetting. Equation (17) implies that I_{23} is a function of I_{13}, α_{s} and D_{s} as introduced and discussed previously. Hence, the value of I_{23} can be readily calculated in this alternative approach.

The variables I_{31}, I_{32} and I_{33} are all governed by the stress-dependent water retention behaviour. The water retention model of Zhou and Ng [61] is used to derive these three variables. The variable I_{31} in equation (1) can be determined as below:

$$I_{31} = \frac{\partial S_{\mathrm{r}}}{\partial e}(1+e) I_{11} + \frac{\partial S_{\mathrm{r}}}{\partial \xi_m} \frac{\partial \xi_m}{\partial p} \quad (18)$$

where ξ_{m} is the ratio between the volume of micro-pores (V_M) to the total volume of pores (V_T) which characterises the pore size distribution (PSD).

The variable I_{32} in equation (1) can be determined using the following equation:

$$I_{32} = \frac{\partial \left[1 + \left(s \frac{e^{m_4}}{m_3} \left(\frac{\xi_{\mathrm{m}}}{\xi_0}\right)^{-m_{\mathrm{m}}}\right)^{m_2}\right]^{-m_1}}{\partial e} D_{\mathrm{q}}(1+e) I_{22} \quad (19)$$

where ξ_0 is the initial value of ξ_{m} before applying any net stress; m_1, m_2, m_3, m_4 and m_{m} are model parameters; D_{q} is the dilatancy associated with the plastic mechanism of shearing. Equation (19) suggests that the value of I_{32} is affected by several factors, including density effects on the SWRC, D_{q} and I_{22}. A lot of data is available in the literature for determining each of them, so I_{32} can be determined based on experimental results readily.

The variable I_{33} in equation (1) can be calculated using the following equation:

$$I_{33} = \frac{\partial \left[1 + \left(s\frac{e^{m_4}}{m_3}\left(\frac{\xi_m}{\xi_0}\right)^{-m_m}\right)^{m_2}\right]^{-m_1}}{\partial s} \quad (20)$$

It should be noted that the value of I_{33} is not constant, but dependent on suction and stress. Moreover, the influence of stress on I_{33} is related to change in the average void ratio and pore size distribution.

3 An extended state-dependent constitutive model for simulating cyclic thermo-hydro-mechanical behaviour of unsaturated soils

3.1 A state-dependent cyclic thermo-hydro-mechanical model

Based on the unified framework expressed by equation (1), this section presents a cyclic thermal-hydro-mechanical model for modelling the state-dependent behaviour of unsaturated soils considering thermal effects. Due to the page limit, only key concepts and formulations are presented in this paper. Further details can be found from Ng et al. [62] and Zhang [63].

The bounding surface plasticity [64] is adopted for capturing elasto-plastic behaviour. The incremental strain components induced by mechanical loading can be readily determined using equations (12) to (20). It should also be noted that, despite the fact that these equations can be adopted, temperature (T) can affect the value of material parameters in those equations. The incremental stain components only induced by thermal loading ($d\varepsilon_v^{th}, d\varepsilon_d^{th}, dS_r^{th}$) can be determined as below:

$$\begin{cases} d\varepsilon_v^{th} = d\varepsilon_v^{the} + d\varepsilon_v^{thp} \\ d\varepsilon_d^{th} = d\varepsilon_d^{the} + d\varepsilon_d^{thp} \\ dS_r^{th} = dS_r^{the} + dS_r^{thp} \end{cases} \quad (21)$$

In the above equation, $d\varepsilon_v^{the}$ is the incremental elastic volumetric strain induced by thermal loading related to thermal expansion coefficient (μ_s), defined as $\frac{\mu_s}{1+e}dT$. The incremental elastic deviator strain and degree of saturation induced by thermal loading (denoted as $d\varepsilon_d^{the}$ and dS_r^{the}, respectively) are assumed to be zero.

To capture the thermo-plasticity under cyclic thermal loading, the memory surface is introduced in addition to loading and bounding surfaces [65] as shown in Figure 1. It is assumed to have the same shape as the bounding surface, and its size is controlled by the memory pressure p_m, which records the maximum stress state of soil.

In this model, the radial mapping rule is used to project the current stress state onto the double surfaces and hence define the image stress states as shown in Figure 1. This simple radial-mapping rule was demonstrated to be effective for many stress paths [64]. The projection centre is assumed to be Point O. Points $A\,(p,q)$, $B\,(\overline{p}_m,\overline{q}_m)$, and $C\,(\overline{p}_b,\overline{q}_b)$ are the current stress state on the loading surface, the image stress state on the memory surface, and the image stress state on the bounding surface, respectively. Based on the Euclidian distances between these points, the mapping rule can be expressed by the following two ratios, which are related to the flow rule and hardening law:

$$\frac{\rho}{\overline{\rho}_b} = \frac{p}{\overline{p}_b} = \frac{q}{\overline{q}_b} \quad (22)$$

$$\frac{\overline{\rho}_m}{\overline{\rho}_b} = \frac{\overline{p}_m}{\overline{p}_b} = \frac{\overline{q}_m}{\overline{q}_b} \quad (23)$$

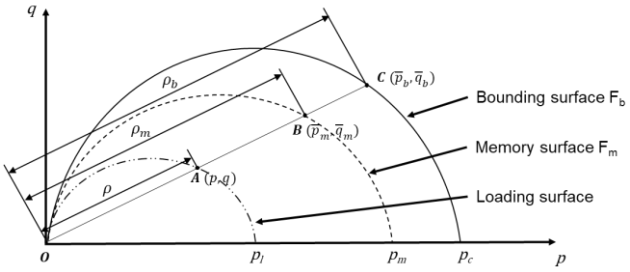

Fig. 1. Bounding surface, memory surface, and loading surface in the $p-q$ plane.

Based on the bounding surface plasticity along with the above mapping rule, the incremental plastic volumetric and deviator strains induced by thermal loading (denoted as $d\varepsilon_v^{thp}$ and $d\varepsilon_d^{thp}$, respectively) can be determined as below:

$$\begin{cases} d\varepsilon_v^{thp} = D_q d\varepsilon_d^{thp} \\ d\varepsilon_d^{thp} = \frac{1}{K_p}\left(\frac{\partial F_b}{\partial p_0}\frac{\partial p_0}{\partial T} + \frac{\partial F_b}{\partial r}\frac{\partial r}{\partial T}\right)dT \end{cases} \quad (24)$$

where F_b is the expression of bounding surface (also illustrated by Figure 1), which is a function of preconsolidation pressure (p_c) and material variable (r) controlling relative distance between normally consolidation line and critical state line. K_p is plastic modulus which involves two ratios defined in the mapping rule (see Eq. (22) and (23)) for the soil stress state within the bounding surface. $\overline{\rho}_b/\rho$ gradually reduces to 1 when the soil stress state moves towards the bounding surface, and the soil behaviour becomes more plastic. Thus, it is used to account for the degradation of soil stiffness during monotonic loading. $\overline{\rho}_b/\overline{\rho}_m$ indicates soil-history-related cyclic loading. This ratio is 1 for soil under monotonic loading or the first cycle of loading, while it is greater than 1 for the following cycles of loading, which decreases the rate of plastic strain accumulation as the number of cycles increases.

3.2 Advanced apparatus for testing unsaturated soil

Figure 2 shows a schematic diagram for the self-developed apparatus for testing volume change of unsaturated soil with suction and temperature control. An open-ended and bottle-shaped inner cell is used inside a conventional triaxial cell. To measure the overall volume change in the specimen, a high-accuracy differential pressure transducer is connected to the inner cell and to a reference tube to record changes in differential pressures between the water pressure change inside the inner cell due to a volume change in the specimen and the constant water pressure in the reference tube [66].

To test unsaturated soils, the axis-translation technique [30] was employed to control matric suction and prevent cavitation. This requires the control of pore-air pressure and pore-water pressure in a soil specimen. The pore-air pressure is applied at the top of the specimen through a coarse porous filter. The pore-water pressure is applied and measured at the base of the specimen through a 5-bar high air-entry ceramic disc. The use of the high air entry value ceramic disc allows the passage of water but prevents the flow of free air from the specimen to the water control and drainage system underneath it.

To control suction and temperature independently in unsaturated soils, the double-cell triaxial apparatus was modified by adding a temperature control system [67]. The temperature control system includes a heating/cooling bath connected with a spiral copper tube installed between the inner cell and the outer cell. The heating/cooling bath mainly consists of a digital controller, a thermostat, a heating/cooling unit, a water bath, an inbuilt pump and a thermocouple. To monitor the temperature, a thermocouple is installed within the water of the inner cell to give feedback to the thermostat and the advanced digital controller. This will then automatically adjust the output of the heating/cooling unit according to the target temperature. Furthermore, a thermal insulating material is used to wrap the whole triaxial apparatus to minimise any heat loss and exchange with the surroundings.

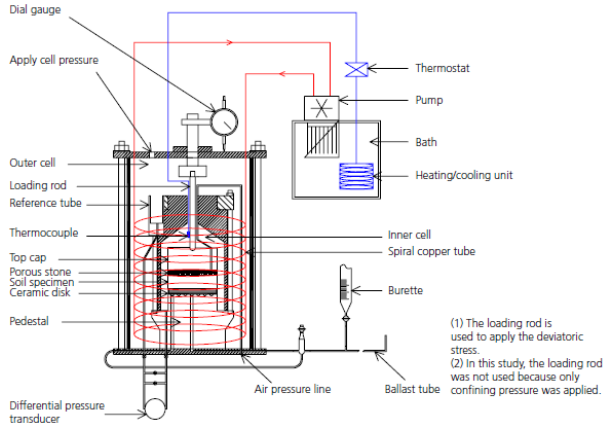

Fig. 2. Double cell apparatus of total volume change measurement with suction and temperature control [67].

3.3 Experimental verification

Figure 3(a) shows the measured response of reconstituted loess under cyclic heating and cooling [68]. A volumetric strain of about 0·45% is induced by the first cycle. With increasing number of cycles, the irreversible strain accumulates, but at a decreasing rate. After five thermal cycles, the accumulated strain is about 0·85%. The computed results are shown in Fig. 3(b) for comparison. It is clear that measured and computed results are matched reasonably well, suggesting that the model can capture the cyclic thermal behaviour of reconstituted soil.

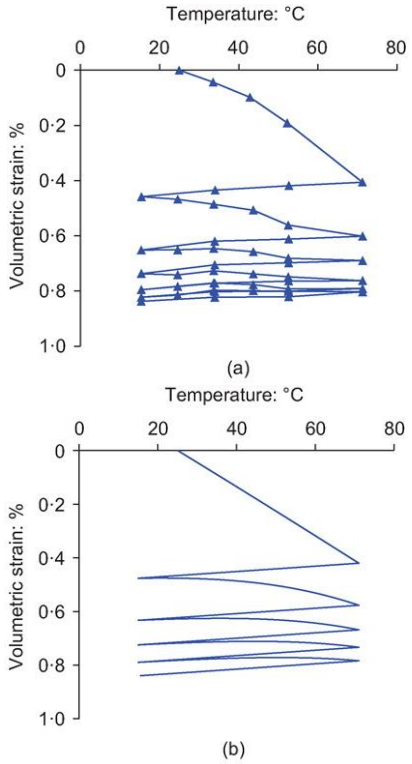

Fig. 3. (a) Measured [68] and (b) computed volumetric strain of saturated soil during thermal cycles.

Figure 4 shows the influence of suction on the volumetric strains during heating and cooling, as determined from both the computed and measured results [67]. During heating, the thermally induced volumetric contraction at zero suction is larger than that at 100 kPa suction; this is due to suction hardening behaviour, which increases the preconsolidation pressure at higher suctions (i.e., 100 kPa). The plastic modulus increases as the difference between the soil state history (reflected by the bounding surface) and the current soil state (reflected by the loading surface) increases, due to suction hardening. The influence of suction hardening on thermally induced volumetric strain was also observed by Romero et al. [69], who tested Boom clay at two suctions.

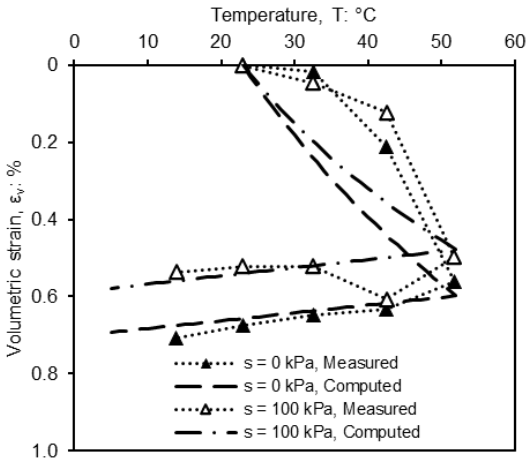

Fig. 4. Measured [67] and computed volumetric strains of unsaturated soil during heating and cooling.

4 Geotechnical applications

4.1 Energy piles under cyclic heating-cooling

The advanced constitutive model is adopted in the back analysis of a centrifuge test on the freestanding energy pile group subjected to asymmetric heating and cooling cycles in the lightly overconsolidated clay (OCR=1.7) with a g-level of 40g [70]. Figure 5 illustrates the experimental model setup. In the centrifuge test, the soil model was made of kaolin clay with an average undrained shear strength of 15 kPa. The piles were made of aluminium cylindrical pipes with a total outer diameter, inner diameter and length of 22 mm, 13 mm and 500 mm, respectively. According to the scaling law, the dimensions of the piles in the prototype are 0.88 m in diameter and 20 m in length (L), of which 16.8 m was embedded in the soil. The model piles in groups were installed with 3D spacing in pre-bored holes at 1g as wished-in-place piles. The pile heads were firmly fixed to the aluminium cap. The working load was 350 N in the model scale (or 560 kN in the prototype) [70], corresponding to half of the pile capacity.

Figure 6 compares the thermally induced displacements of energy pile EP1 obtained from numerical simulation with those from the centrifuge test. The term 'thermally induced' means that mechanical load-induced displacement has been subtracted. In the figure, the pile head settlement (w) is normalised by the pile diameter (D). The positive and negative values denote settlement and heave, respectively. At the end of the 10th thermal cycle, the thermally induced settlement of EP1 exceeds the criterion of Ng et al. [71] and Eurocode 7 [72]. It can be seen that the ratcheting pattern is observed in both experimental results and THM simulations. This consistency indicates that the irreversible pile head displacement is captured well by the FE model. The existing numerical studies used elasticity (e.g., [73, 74] etc.) or the MC soil model (e.g., [75, 76] etc.), which might lead to the thermally induced settlement being underestimated for energy piles constructed in normally consolidated or lightly overconsolidated clay [77] if thermo-plasticity occurs. However, the thermo-elastic constitutive relationships are valuable and reasonable to simulate the behaviour of energy geostructures in dense sands and heavily overconsolidated soils in both symmetric and asymmetric cases. By using appropriate parameters in the thermo-elastic soil models, the simulation procedures could be simplified. In these cases, the results of the irreversible settlement and group tilting in the numerical simulation are small and consistent with the field tests of energy piles in dense sand and stiff clay [78, 79].

Figure 7 shows the thermally induced unit shaft resistance of the energy pile EP1. The shaft resistance caused by mechanical load was subtracted initially. The unit shaft resistance is obtained from the shear stress at the pile–soil interface along the pile shaft in Abaqus, which is defined as positive in an upward direction. In the first heating phase, the increase in temperature of EP1 leads to negative shaft resistance for locations between z=0 and z=12·5 m, and a positive shaft resistance between z=12·5 m and z=16·8 m. The energy pile lengthens, and its shallow parts move upwards, while the plastic contraction of soil induces settlement in the shallow soil layer. It is known that any axial deformation will be opposed by shaft restraint at the pile–soil interface [80]. Hence, this relative movement of pile and soil leads to negative shear stress.

.

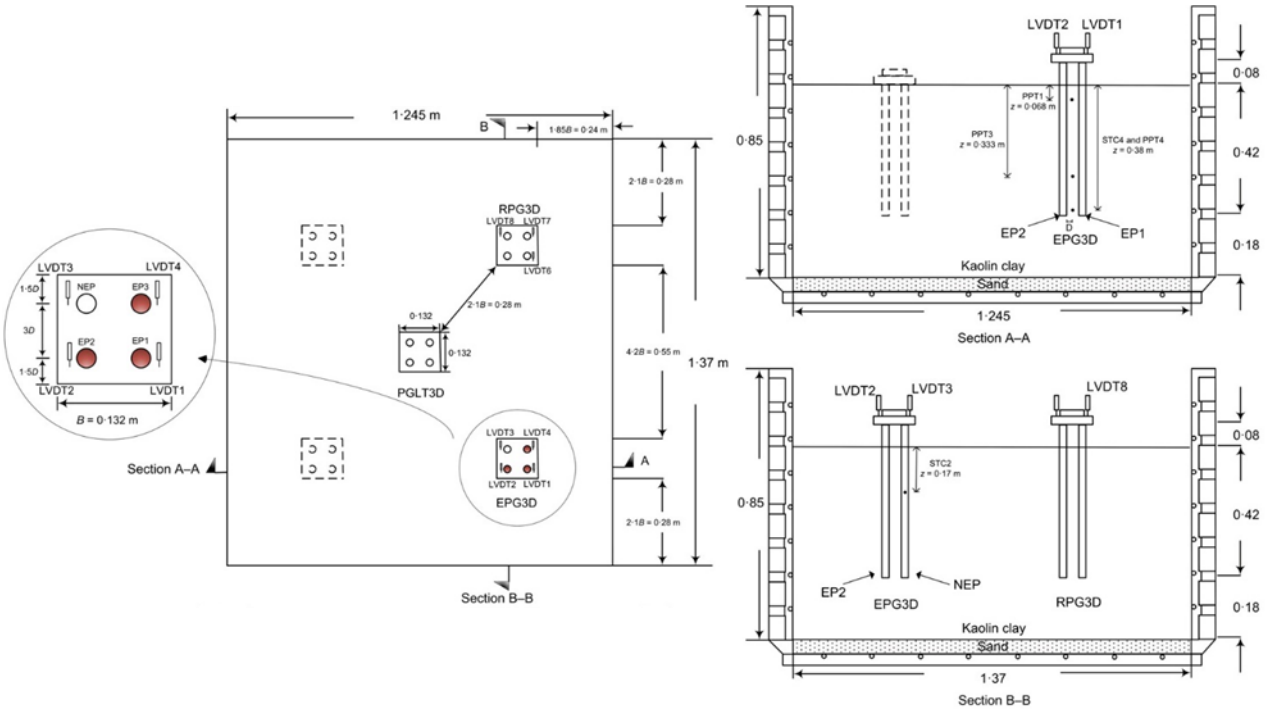

Fig. 5. Model setup of centrifuge tests of energy pile groups (after Ng et al. [70]).

For the floating energy pile in this study, the lower half of the energy pile moves downwards because of heating expansion, leading to positive shaft resistance. In contrast, the response reverses when the pile is cooled, as the relative movement in the cooling phase is opposite to that in the heating phase. Further, it can be found that the shaft resistance decreases with increasing thermal cycles. This is because of the loss of confining pressure in the surrounding soil, which can be estimated as [81]

$$\tau_s = (\sigma_h' \pm \Delta\sigma_h') \tan\theta \qquad (25)$$

where θ is the contact angle at the pile–soil interface. The toe resistance of the energy piles is thereby mobilised to compensate for the decrease in shaft resistance, which eventually leads to the settlement of the energy pile.

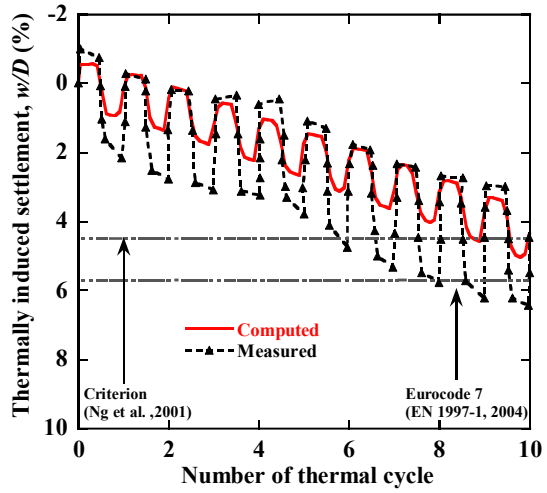

Fig. 6. Comparison between measured [70] and computed results of thermally induced pile head settlement。

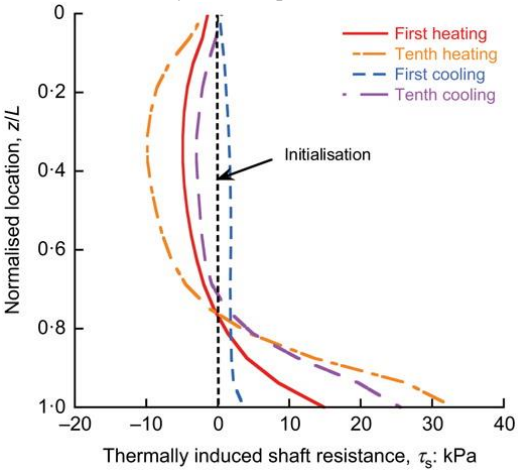

Fig. 7. Mobilisation of shaft resistance at the pile–soil interface of energy pile.

4.2 A 15-m deep excavation in Tianjin, China

The suction-dependent small-strain soil stiffness is adopted in the analysis of a 15-m deep excavation in the downtown area of Tianjin, China. The excavation project for the high-rise buildings is approximately 181 m by 268 m on plane. The northern side was retained by 29 m-long contiguous piles (each diameter of 0.9 m at 1.1 m spacing), whereas the other three sides were supported by diaphragm walls with a thickness of 1–1.2 m. In the northern side, an earth berm (19 m in width and 11.5 m in height) was cut in front of the pile wall to provide extra support during excavation (Figure 8 (a)). At the inner boundary of the earth berm, two-row 21 m-long contiguous piles with row spacing of 3.2 m were installed (Figure 8 (b)).

In the excavation site, there were three different soil types (i.e., fill, silt and silty clay) along the depth (Figure 8 (b)). The top 5.5 m layer was fill material. The soil at depths of 9.5–11.5 m and 23.0–24.2 m was classified as silt. Soil at other depths was classified as silty clay. In order to determine the basic properties of the soils, intact soil samples were collected from the field for laboratory triaxial and oedometric tests [82]. The parameters used in the simulation were determined based on the experimental data by the least-squares method using a multiple linear regression model.

The simulation procedures were in accordance with the actual construction stages. The initial stress conditions of soils in the simulation were generated at 1 g (gravitational acceleration) by assuming that the coefficient of at-rest earth pressure of soil (K_0) is equal to 1 – sinφ'. At construction Stage 1, the installation of the contiguous piles was modelled with a "wish-in-place" (WIP) wall for simplicity [83]. Then, the plate elements of the contiguous piles were activated. At Stage 2, water table inside the excavation was lowered down to the depth of −17.2 m. From Stage 3 to Stage 6 (final stage), the ground was consecutively excavated to the depths of −2 m, −3.7 m, −10.45 m and −15.2 m, respectively. The suction distribution above the ground water table during excavation was assumed to follow the hydrostatic line. Excavation was simulated by removing nodes and elements in each stage.

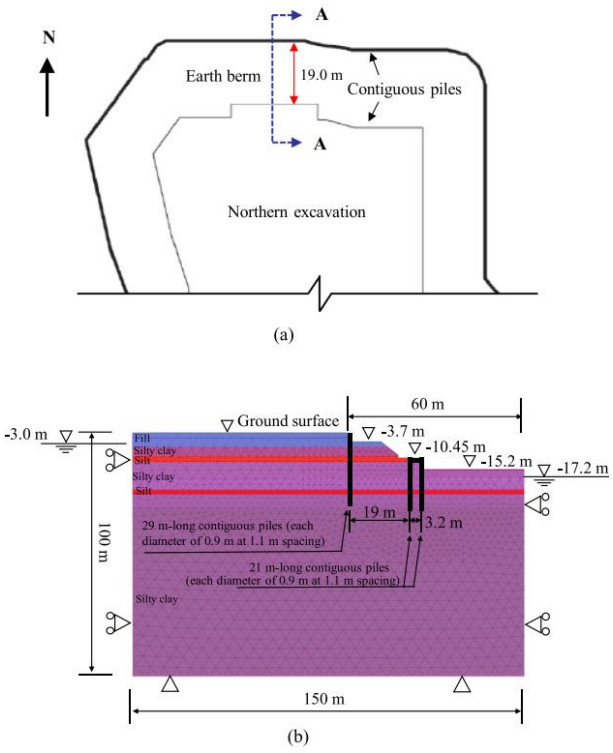

Fig. 8. (a) Location of cross-section A-A (plan view) and (b) cross-section A-A of the excavation used in the design analysis.

Figure 9(a) shows the comparison of the measured and predicted wall deflection without considering suction effects on small-strain soil stiffness. It can be seen that a cantilever mode of wall deflection was measured and predicted after each excavation stage. From construction Stage 3 to the final stage, the magnitude of wall deflection increased, especially near the ground surface. The measured maximum lateral wall deflection was around 0.3% of excavation depth. This value is much smaller than Peck's data (2% of excavation depth; Peck [84]), where there were lateral supporting systems. It implies that without using the lateral supporting systems in the current project, the presence of unsaturated earth berm in front of pile wall could also reduce the wall deflection significantly.

The analysis without considering unsaturated soil stiffness shows that the predicted results were larger than the measured data, especially at Stage 5 and final stage. At the end of excavation, wall deflection near ground surface was overestimated by 85%. However, the prediction used to control construction was improved significantly when considering the effects of soil suction on soil stiffness in the model (Figure 9(b)). The analysis considering soil suction effects predicted the wall deflection quite well at Stage 3. The prediction error was only 20% at the final stage. The comparison between Figure 9(a) and (b) reveals that the wall deflection was highly overestimated when soil stiffness was determined from saturated soils. It also demonstrates the importance of modelling suction-dependent small-strain soil stiffness in the design analysis of deep excavations.

Figure 10 shows the basement heave during excavation. The measured maximum heave was 43 mm, which was around 4 m away from the inner pile wall. The predicted results clearly show that the basement heave was in convex shape, with the maximum value at about 3 m away from the pile wall. The heave amount became constant, when the distance away from the pile wall was more than 20 m. Compared to the analysis based on saturated soil stiffness, the analysis considering suction-dependent soil stiffness could better predict the maximum basement heave. The accuracy of prediction was improved by more than 40%, when suction effects were considered. This improvement demonstrates that the unsaturated soil within the top 2 m of the basement could restrict the ground heave due to the suction induced increase in small-strain soil stiffness.

After considering the suction effects on maximum shear modulus, the trends of wall deflection and basement heave remained similar. Besides, the locations of the maximum basement heave did not change. This observation is consistent with the measured results reported by Roy and Robinson [85] and Zhang et al. [86], who showed that the locations of peak ground movements were not affected by the changes in effective stress due to dewatering. Based on the predicted and measured results in Figure 9 and Figure 10, it is clear that the design analysis with suction-dependent small-strain soil stiffness properly predicted the field performance due to de-watering in deep excavation. Hence, the analysis considering unsaturated soil stiffness provided a safe and economical design during construction. It saved construction time and reduced construction costs Ng et al. [87].

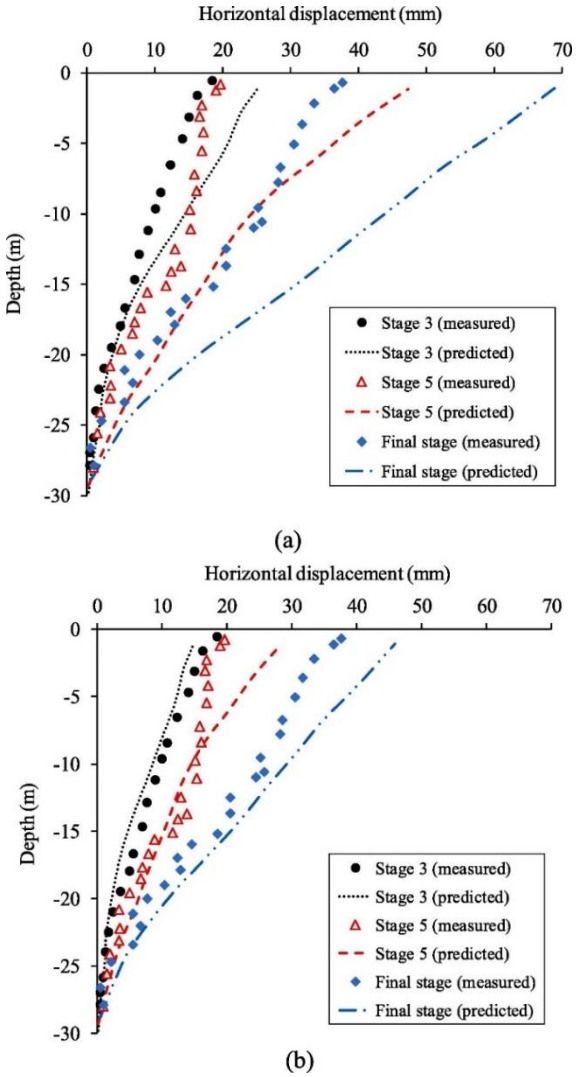

Fig. 9. Comparison between measured and predicted displacement of pile wall: (a) without and (b) with considering suction-dependent soil stiffness.

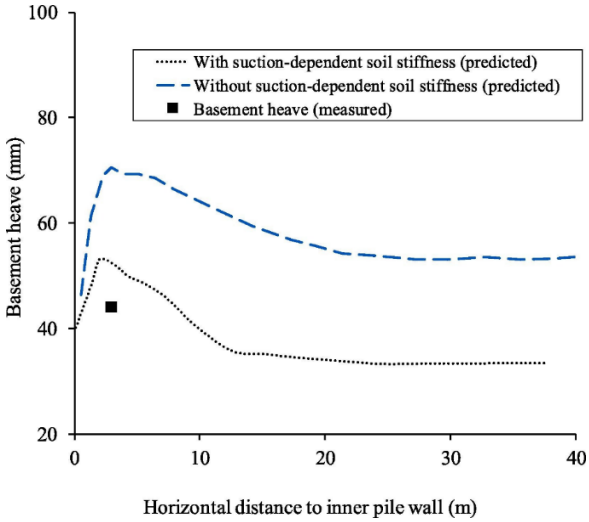

Fig. 10. Comparison between measured and predicted basement heave with and without considering suction-dependent soil stiffness.

5 Conclusions

In this plenary lecture, a unified state-dependent theoretical framework in the form compliance matrix has been described to simulate the state-dependent hydro-mechanical behaviour of unsaturated soil. This framework uses mean net stress, deviator stress and suction as state-dependent constitutive stress variables. The nine state-dependent variables, which have clear physical meanings, in the compliance matrix were derived. Based on the theoretical framework, a new state-dependent cyclic thermo-hydro-mechanical model was developed and reported. By using the new theoretical model, two geotechnical engineering applications were analysed including cyclic thermally loaded floating energy pile foundations and a deep excavation in unsaturated ground. Consistent results are obtained between analysed and measured data. It is evident that the newly developed state-dependent model is capable to simulate various types of engineering problems such as cyclic thermally loaded energy piles and deep excavations in both saturated and unsaturated soils. Also this state-dependent framework can be extended to simulate soil-plant interactions [88].

Acknowledgement

The authors would like to thank the Research Grants Council (RGC) of the Hong Kong Special Administrative Region, China for providing financial support through the grants 16204817, 16207819 and AoE/E-603/18.

References

1. D.G. Fredlund, H. Rahardjo, Soil mechanics for unsaturated soils. New York: John Wiley & Sons, (1993)
2. C.W.W. Ng, B.K. Menzies, Advanced unsaturated soil mechanics and engineering. London and New York: Taylor & Francis (2007)
3. C.W.W. Ng, C. Zhou, C.F. Chiu, Acta Geotech. **15**, 2705-2725 (2020)
4. E.E. Alonso, A. Gens, A. Josa, Géotechnique **40**, 405-430 (1990)
5. R. Chen, Y. Ge, Z. Chen, J. Liu, Y. Zhao, Z. Li, J. Hydro. **568**, 260-274 (2019)
6. Y. Gao, D. Sun, Z. Zhu, Y. Xu, Acta Geotech. **14**, 417-428 (2019)
7. M. Lloret-Cabot, S.J. Wheeler, J.A. Pineda, E. Romero, D. Sheng, Acta Geotech. **13**, 15-37 (2018)
8. C.W.W. Ng, C. Zhou, Géotechnique **64**, 709-720 (2014)
9. C.W.W. Ng, C. Zhou, Q. Yuan, J. Xu, Can. Geotech. J. **50**, 223-232 (2013)
10. D. Sheng, S.W. Sloan, A. Gens, Comput. Mech. **33**, 453-465 (2004)
11. D. Sun, D. Sheng, S.W. Sloan, Mech. Mater. **39**, 212-221 (2007)
12. S.J. Wheeler, R.S. Sharma, M.S.R. Buisson, Géotechnique **53**, 41-54 (2003)
13. Y.L. Xiong, G.L. Ye, Y. Xie, B. Ye, S. Zhang, F. Zhang. Acta Geotech. **14**, 313-328 (2019)
14. A.N. Zhou, D. Sheng, S.W. Sloan, A. Gens, Comput. Geotech. **43**, 111-123 (2012)
15. A.N. Zhou, D. Sheng, S.W. Sloan, A. Gens, Comput. Geotech. **43**, 178-187 (2012)
16. C. Zhou, C.W.W. Ng, Géotechnique **66**, 344-350 (2016)
17. D.G. Toll, Géotechnique **40**, 1, 31-44 (1990)
18. X. Zhang, E.E. Alonso, F. Casini, Comput. Geotech. **71**, 56-68 (2016)
19. D. Gallipoli, S.J. Wheeler, M. Karstunen, Géotechnique **53**, 1, 105-112 (2003)
20. D. Gallipoli, A. Gens, R. Sharma, J. Vaunat, Géotechnique **53**, 1, 123-135 (2003)
21. R.I. Borja, Comput. Method Appl. M. **193**, 48-51, 5301-5338 (2004)
22. E.E. Alonso, J.M. Pereira, J. Vaunat, S. Olivella, Géotechnique **60**, 12, 913-925 (2010)
23. B. François, L. Laloui, Int. J. Numer. Anal. Met., **32**, 16, 1955-1988 (2008)
24. W. Sun, D. A. Sun, Int. J. Numer. Anal. Met. **36**, 8, 1002-1022 (2012)
25. D. Mašín, N. Khalili, Int. J. Numer. Anal. Met. **36**, 12, 1461-1485 (2012)
26. Y. Tang, W. Wu, K. Yin, S. Wang, G. Lei, Comput. Geotech. **112**, 284-292 (2019)
27. Y. Liu, G. Cai, A. Zhou, B. Han, J. Li, C. Zhao, Comput. Geotech. **133**, 104032 (2021)
28. B.I. Donald, A.W. Bishop, The experimental study of partly saturated soil in the triaxial apparatus. In Proceedings of the 5th international conference on soil mechanics and foundation engineering, Paris, France (1961)
29. D. Croney, Suction of moisture held in soil and other porous materials. (1952)
30. J.W. Hilf, An investigation of pore water pressure in compacted cohesive soils, In Technical Memo 654, Denver: US Bureau of Reclamation (1956)
31. A. Tarantino, L. Mongiovì, G. Bosco, Géotechnique, **50**, 3, 275-282 (2000)
32. M. Caruso, A. Tarantino, Géotechnique, **54**, 4, 281-284 (2004)
33. C.W.W. Ng, Y.J. Cui, R. Chen, P. Delage, Soils Found. **47**, 675-684 (2007)
34. C.W.W. Ng, C. Zhou, A.K. Leung, Vadose Zone J. **14**, vzj2015.2001.0006 (2015)
35. A.M. Tang, Y.J. Cui, N. Barnel, Géotechnique, **58**,1, 45-54 (2008)
36. A. Khosravi, J. S. A., & McCartney, J. S. (2012). J. Geotech. Geoenviron. **138**, 11, 1326-1333 (2012)
37. N.A. Alsherif, J.S. McCartney, Géotechnique, **65**, 9, 703-716 (2015)

38. Y. Gao, D.A. Sun, A. Zhou, Can. Geotech. J. **53**, 6, 909-917 (2016)
39. F. D'Onza, D. Gallipoli, S.J. Wheeler, F. Casini, J. Vaunat, N. Khalili, L. Laloui, C. Mancuso, D. Masin, M. Nuth, J.M. Pereira, R. Vassallo, Géotechnique **61**, 283-302 (2011)
40. A. Gens, M. Sánchez, D. Sheng, Acta Geotech. **1**, 137 (2006)
41. D. Sheng, Comput. Geotech. **38**, 757-776 (2011)
42. D. Sheng, A. Gens, D.G. Fredlund DG, S.W. Sloan, Comput. Geotech. **35**, 810-824 (2008)
43. R.I. Borja, A. Koliji, J. Mech. Phys. Solids, **57**, 8, 1182-1193 (2009)
44. S.J. Wheeler, D. Karube, Constitutive modelling. In Proceedings of the First International Conference on Unsaturated Soil, 6-8 September 1996, Paris, France (1996).
45. N. Khalili, F. Geiser, G.E. Blight, Int. J. Geomech. **4**, 2, 115-126 (2004)
46. N. Khalili, E. Romero, F.A. Marinho, State of the Art Report. Advances in Unsaturated Soil Mechanics: Constitutive modelling, experimental investigation, and field instrumentation. In Proceedings of the 20th ICSMGE-State of the Art and Invited Lectures—Rahman and Jaksa, Sydney, Australia, 1-5 (2022)
47. C.W.W. Ng, X. Zhao, S. Zhang, J. Ni, C. Zhou, Géotechnique 1-20 (2022)
48. C.W.W. Ng, G. Zheng, J. Ni, C. Zhou, Comput. Geotech. **119**, 103375 (2020)
49. X. Duan, L. Zeng, X. Sun, Acta Geotech. **14**, 5,1459-1481 (2019)
50. A. Russell, N. Khalili, Int. J. Numer. Anal. Met. **30**, 3, 181-212 (2006)
51. R. Chen, Experimental study and constitutive modelling of stress-dependent coupled hydraulic hysteresis and mechanical behaviour of an unsaturated soil. PhD thesis, Hong Kong University of Science and Technology (2007)
52. N. Khalili, M. Habte, S. Zargarbashi, Comput. Geotech. **35**, 6, 872-889 (2008)
53. N. Khalili, M.H. Khabbaz, Géotechnique **48**, 5, 681-687 (1998)
54. N. Lu, J.W. Godt, D.T. Wu, Water Resour. Res. **46**, 5 (2010)
55. N. Lu, W.J. Likos, J. Geotech. Geoenviron. Eng. **132**, 2, 131-142 (2006)
56. C.F. Chiu, C.W.W. Ng, Géotechnique, **53**, 9, 809-829 (2003)
57. K. Been, M.G. Jefferies, Géotechnique, **35**, 2, 99-112 (1985)
58. D.C. Sheng, D.G. Fredlund, A. Gens, Can. Geotech. J. **45**, 4, 511-534 (2008)
59. C.W.W. Ng, S.Y. Yung, Géotechnique, **58**, 1, 23-35 (2008)
60. P. Vardanega, M. Bolton, J. Geotech. Geoenviron. **139**, 9, 1575-1589 (2013)
61. C. Zhou, C.W.W. Ng, Comput. Geotech. **62**, 216-222 (2014)
62. C.W.W. Ng, Q. Zhang, S. Zhang, S.Y. Lau, H. Guo, Z. Li, Géotechnique (under review)
63. Q. Zhang, Cyclic thermo-hydro-mechanical behaviour of vegetated soil slope under climate change: constitutive and numerical modelling, PhD thesis, Hong Kong University of Science and Technology (under preparation)
64. Y.F. Dafalias, J. Eng. Mech. **112**, 9, 966-987 (1986)
65. C. Zhou, K.Y. Fong, C.W.W. Ng, Int. J. Numer. Anal. Met. **41**, 16, 1655-1666 (2017)
66. C.W.W. Ng, L.T. Zhan, Y.J. Cui, Can. Geotech. J. **39**, 3, 757-764 (2002)
67. C.W.W. Ng, Q. Cheng, C. Zhou, E.E. Alonso, Géotech. Lett. **6**, 3, 192-198 (2016)
68. C.W.W. Ng, Q.Y. Mu, C. Zhou, Géotechnique, **69**, 2, 146-150 (2019)
69. E. Romero, A. Gens, A. Lloret, Géotechnique **53**, 1, 65-81 (2003)
70. C.W.W. Ng, A. Farivar, S.M.M.H. Gomaa, M. Shakeel, F. Jafarzadeh, Renew. Energ. **172,** 998-1012 (2021)
71. C.W.W. Ng, T.L.Y. Yau, J.H.M. Li, W.H. Tang, J. Geotech. Geoenviron. **127**, 6, 488-498 (2001)
72. En1997-1, Eurocode 7: Geotechnical Design - Part 1: General rules [Authority: the European Union Per Regulation 305/2011, Directive 98/34/EC, Directive 2004/18/EC] (2004)
73. A.F. Rotta Loria, L. Laloui, Géotechnique. **68,** 9, 834-841 (2018)
74. D. Wu, H. Liu, G. Kong, A.F. Rotta Loria, Can. Geotech. J. **58,** 11, 1757-1769 (2021)
75. A. Di Donna, A.F. Rotta Loria, L. Laloui, Comput. Geotech. **72,** 126-142 (2016)
76. K. Sarma, R. Saggu, J. Geotech. Geoenviron. **146,** 11, 04020114 (2020)
77. H.M. Abuel-Naga, D.T. Bergado, A. Bouazza, G.V. Ramana, Can. Geotech. J. **44,** 8, 942-956 (2007)
78. P.J. Bourne-Webb, B. Amatya, K. Soga, T. Amis, C. Davidson, P. Payne, Géotechnique. **59,** 3, 237-248 (2009)
79. B. Wang, A. Bouazza, R.M. Singh, C. Haberfield, D. Barry-Macaulay, S. Baycan, J. Geotech. Geoenviron. **141,** 4, 04014125 (2015)
80. B.L. Amatya, K. Soga, P.J. Bourne-Webb, T. Amis, L. Laloui, Géotechnique. **62,** 6, 503-519 (2012)
81. C.W.W. Ng, C. Shi, A. Gunawan, L. Laloui, H.L. Liu, Can. Geotech. J. **52,** 8, 1045-1057 (2015)
82. G. Zheng, X. Yang, H. Zhou, Y. Du, J. Sun, X. Yu, Comput. Geotech. **95**, 119–28 (2018)
83. C.W.W. Ng, Nonlinear modelling of wall installation effects. In Proceeding of International

Conference on Retaining Structures, London, England (1992)

84. R.B. Peck. Deep excavation and tunnelling in soft ground, in Proceedings of the 7th international conference on soil mechanics and foundation engineering, state-of-the-art volume, Mexico City, (1969)
85. D. Roy, K.E. Robinson, Eng. Geol. **107**, 3–4, 109–117 (2009)
86. Y.Q. Zhang, J.H. Wang, M.G. Li, Int. J. Geomech. **18**, 10, 04018120 (2018)
87. C.W.W. Ng, N. Simons, B. Menzies, Soil-structure engineering of deep foundations, excavations and tunnels. London: Thomas Telford, (2004)
88. C.W.W. Ng, A.K. Leung, J. Ni, Plant-soil slope interaction. London and New York: Taylor & Francis (2019)